Invited paper

Optoelectronic integrated devices Part II. Advanced optical functions and surface-emitting capability

S. NODA[1]* and A. SASAKI[2]

[1] Department of Electronic Science and Engineering, Kyoto, Japan
[2] Osaka Electro-Communication University, Neyagawa, Japan

Following the previous paper "Optoelectronic Integrated Devices: Part I. Principle, Technology, and Applications" [1], new developments of the integrated devices are described. The devices have been fabricated based on the concept that the higher the degree of integration, the higher the functionality of the device. The advanced optical logic-functions such as various flip-flops are demonstrated. The trial to let the integrated devices possess the surface-emitting function without loss of the functionality is also described, which is very important to obtain two-dimensional arrays of functional devices.

1. Introduction

Optoelectronic integrated devices (OEIDs) [1–3], in which light-receiving and light–emitting devices are vertically and directly integrated, produce various new optical functions important for optical signal processing and optical interconnections. The principle, technology, and applications of the OEIDs were recently reported in the paper: "Optoelectronic Integrated Devices: Part I" published in this journal [2]. The paper indicates that by integrating vertically and directly conventional optoelectronic devices, not only the combined characteristics of the constituent devices, but also new functions due to the mutual interaction between them can be easily obtained. This leads to more general engineering concept that the higher the degree of integration, the higher the functionality of the device. We demonstrate in this paper advanced optical logic-devices with various flip-flop functions by integrating multiple laser diodes (LDs) and heterojunction phototransistors (HPTs) and utilizing internal optical and electrical couplings.

In the application of the integrated devices to parallel signal processings, it is very important to possess a surface-emitting function. Recently, a vertical cavity surface-emitting laser (VCSEL) [4] has been drawing much attention. When we use the VCSEL as the laser part of the integrated devices, however, the optical feedback from the VCSEL to the HPT becomes too strong since the lasing output power directly enters the HPT. As described later, the integrated device utilizes the spontaneous emission instead of the lasing emission as the optical feedback to obtain various functions. The strong optical feedback leads to the limited numbers of functions such as an optical switching. To avoid this limitation, we consider here using a circular grating coupled surface-emitting device [5, 6]. The lasing oscillation occurs in the direction parallel to the substrate surface, and a part of the light is coupled out to the direction normal to the substrate surface. Therefore, when we integrate the HPTs on the position where there is no grating coupler, the feedback light becomes spontaneous light and various functions can be expected.

In the following, we first describe the principle,

* Corresponding address: Dr S. Noda, Department of Electronic Science and Engineering, 606–01 Kyoto, Japan,
Tel: +81-75-753-5297, Fax: +81-75-751-1576,
e-mail: snoda@kuee.kyoto-u.ac.jp

fabrication, and characteristics of the OEIDs with advanced optical logic functions. Then, the trial for the development of the circular grating coupled surface-emitting device applicable to the OEIDs is explained.

2. OEIDs with various optical logic (flip-flop) functions

2.1. Device Structure and Fabrication

The schematic structure of the device developed in this work is shown in Fig. 1 [7]. Six HPTs are integrated vertically and directly on two LDs. Among six HPTs, the HPT-A and the HPT-B are integrated just above the LD1 stripe, and the HPT-E and the HPT-F are integrated just above the LD2 stripe. The HPT-C and the HPT-D are integrated on the position between the LD1 and the LD2.

The crystal layers for the device were grown by three-step liquid-phase epitaxy (LPE) [3]. The p-InP buffer layer, the current blocking layers of n-InP and p-InP, and the undoped-InGaAsP cap layer were successively grown on a (100) p^+-InP substrate during the first step of LPE. After the formation of the grooves with 1.5μm width and 300μm separation by a photolithography, the p-InP clad, the undoped-InGaAsP active, the n-InP clad, and the n-InGaAsP optical absorptive layers were grown at the second step of LPE. A stripe geometry LD was formed by these growth processes. The HPT part composed of the n-InGaAsP optical absorptive, the n-InP collector, the p-InGaAsP base, and the n-InP emitter layers was grown at the third step of LPE. In the crystal wafer, the wavelengths of the active layer

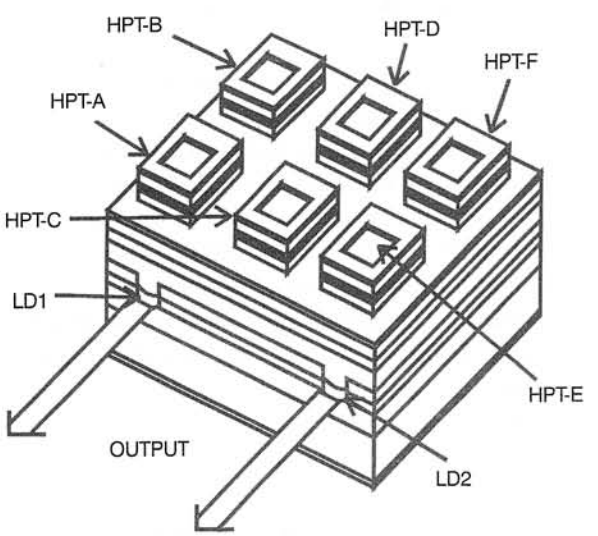

Fig. 1. Schematic structure of OEID with six HPTs and two LDs.

of the LD and the base layer of the HPT were at first intentionally shifted so that the HPT can only respond to the spontaneous emission of the LD to reduce the optical feedback inside the device.

A square-shaped AuGe-Ni-Au electrode was deposited on the epilayer side, and the wafer was mesa-etched down to the collector layer to form six HPTs. The periphery of the HPTs was coated with a polyimide film to avoid the leakage current due to the formation of the surface states. An AuZn-Au electrode was deposited on the back side followed by being sintered in H_2 atmosphere. The wafer was cleaved and bonded on a silver heat sink. The dimension of each HPT mesa was 120×100 μm^2 and the cavity length of the LDs was 400 m.

2.2. Bistable and tristable optical flip-flop functions

Since the integrated device has many components, there are various couplings inside the device in both electrical and optical points of view [7, 8]. By utilizing these internal couplings, we can achieve various functions. The optical flip-flop function is considered especially important for digital optical signal processing. The function can be achieved by the simultaneous utilization of the HPT-A + LD1 and HPT-E + LD2 parts. Figure 2(a) shows the equivalent circuit, where each part is biased through the common load resistance R_c. When the optical input is incident to the HPT-A, the photo-induced current flows through the LD1 and drives it. Since the HPT-A is integrated just above the LD1, a part of the light emitted from the LD1 is fed back to the HPT-A, which induces negative resistance in its current-voltage characteristics. When the optical input to the HPT-A exceeds a threshold level, the HPT-A + LD1 part is switched to the ON-state due to the negative resistance characteristics. In this case, the HPT-E + LD2 part is maintained to the OFF-state but the voltage at the both ends is made small V_{rd}, which is equal to the voltage at the both ends of the HPT-A + LD1 part at the ON-state. When the optical input is incident to the HPT-E + LD2, a part of the current flowing through the HPT-A + LD1 starts to flow through the HPT-E + LD2, since the HPT-E has enough gain even at the reduced voltage V_{rd}. The reduction of the current through the HPT-A + LD1 decreases the optical feedback from the LD1 to the HPT-A and finally the HPT-A + LD1 part looses the optical feedback enough to maintain the ON-state. On the other hand, the increase of the current through the HPT-E + LD2 induces optical feedback enough to let

 © 1997 COSiW SEP, Warsaw

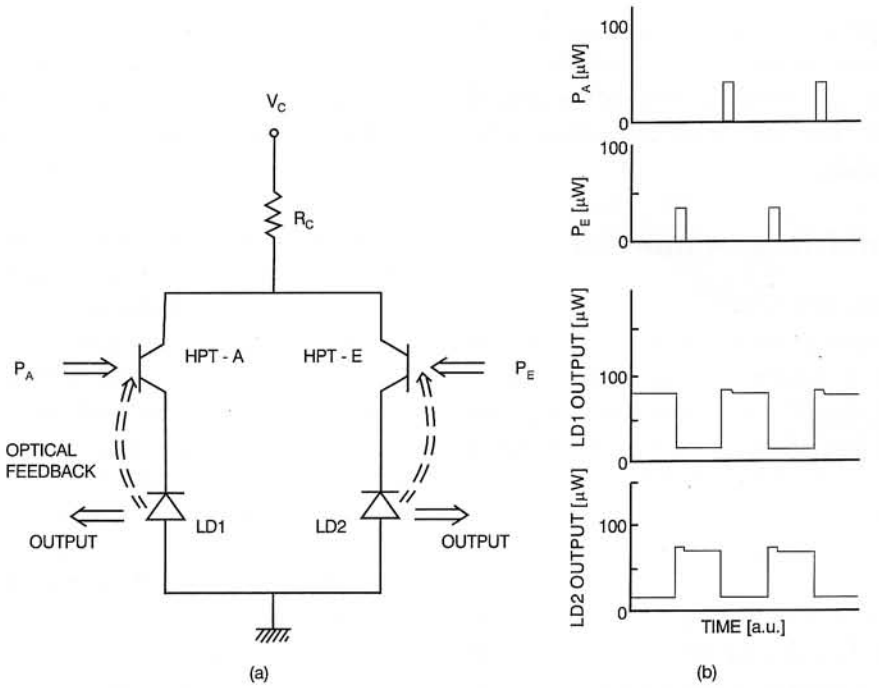

Fig. 2. Equivalent circuit (a) and operation of bistable flip-flop function (b).

this part be switched on. Thus, the state becomes reverse, that is, the HPT-A + LD1 turns to the off-state and the HPT-E + LD2 turns to the on-state. Figure 2(b) shows the resultant flip-flop operation. We can see that the output state has been alternately switched by the alternate optical input to the HPT-E and to the HPT-A, respectively.

This function can be extended to the tristable flip-flop function by using the HPT-B and the HPT-F additionally. The equivalent circuit is shown in Fig. 3(a), where the HPT-A + LD1 and the HPT-F + LD2 parts are biased through a common load resistance R_{c1} and the HPT-B + LD1 and HPT-E + LD2 parts are biased through a common resistance R_{c2}. Due to the parallel connection, only one part which receives higher optical input can be switched on as described above. Here, the optical inputs to the HPT-A and the HPT-E are from external light sources (S,R), and the optical inputs to the HPT-B and the HPT-F are from the HPT-A and HPT-E parts through the LD1 and LD2, respectively [8]. The possible output states of the device are as follows: i)the HPT-A + LD1 and HPT-B + LD1 parts are at the on-states, but the HPT-E + LD2 and HPT-F + LD2 parts are at the off-states, what corresponds to (Q, $\overline{Q}$) = (2, 0); ii)the HPT-A + LD1 and the HPT-E + LD2 are at the on-states, but the HPT-B + LD1 and the HPT-F + LD2 parts are at the off-states, what corresponds to (Q, $\overline{Q}$) = (1,1); and iii)the HPT-E + LD2 and the HPT-F + LD2 are at the on-states, but the HPT-A + LD1 and the HPT-B + LD1 parts are at the

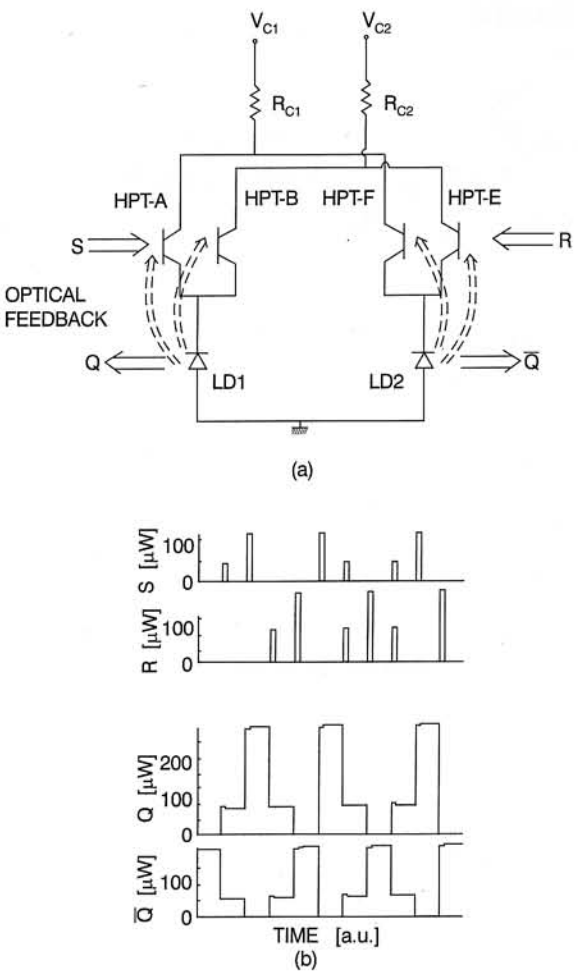

Fig. 3. Equivalent circuit (a) and operation of tristable flip-flop function (b).

off-states, what corresponds to (Q, $\overline{Q}$) = (0,2). Figure 3(b) shows the results obtained experimentally, and we can see that the device indeed exhibited the tristable flip-flop function. The switching time was a few hundreds nanoseconds.

2.3. Astable multivibrator function

In the optical flip-flop function described in Section 2-2, when each output portion is cross-interconnected to the corresponding input portion by optical fibers as shown in Fig.4(a), the self-oscillation can be expected. This is so-called the astable multivibrator function. When the number of the HPT + LD parts is increased and each part is interconnected to the neighboring part sequentially, the self-scanning light-emitter can be expected.

As described in Section 2-1, the wavelengths of the active layer of the LD and the base layer of the HPT were intentionally shifted so that the HPT can respond not to the lasing output light of the LD but only to the spontaneous emission. Therefore, to achieve above interconnection, both wavelengths should be coincided with each other. In this case, the optical feedback from the LD to the HPT is greatly increased (about factor of 10) due to the larger spectral response of the HPT [9]. There are various methods to reduce the optical feedback: (i)reduction of surface-area of each HPT, (ii)insertion of thicker optical absorptive layer between the HPT and the LD, and (iii)shift of the relative position between the LD stripe and the HPT. Although the method (i) is considered best when we take into account that the speed of the device becomes faster, the method (iii) is utilized here from the view point of the process easiness. By the analysis of the optical feedback determined by the geometrical arrangement, we have found that the shift of about 20 μm from the edge of the HPT to the LD stripe is required to achieve the appropriate optical feedback. Based on this knowledge, we have fabricated an integrated device with the same wavelengths of the active and base layers, and made the cross-interconnection as shown in Fig.4(a). The resultant characteristics are shown in Fig.4(b). It can be seen that the astable multivibrator function has been achieved, where the period of the oscillation is determined by the propagation (delay) time of the light through the interconnecting fiber. The reason why so long delay time (about 10ms by 2km-fiber) was utilized is to avoid complicated phenomena caused by the competition between the delay time and the device switching time (about 200ns). In actual operation, we can utilize much shorter optical fiber length: for example 20cm-fiber can be possible if the device speed becomes 1ns. The principle is completely different from the conventional electrical astable multivibrator, where the charging time of the capacitance of the circuit determines the oscillation frequency. When the number of the HPT + LD parts is increased and each part is interconnected to the neighboring part sequentially, the self-scanning light-emitter can be expected.

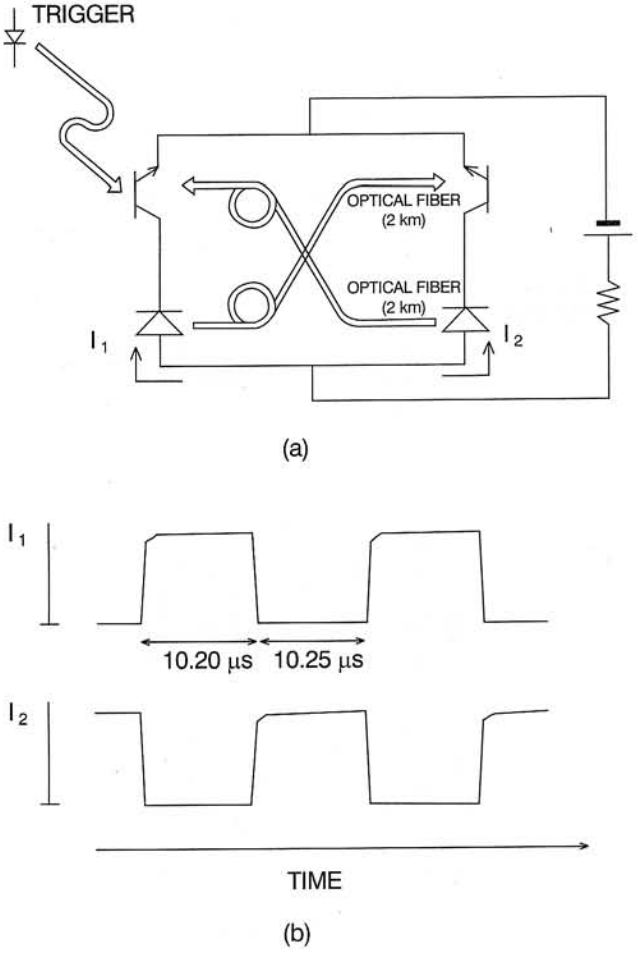

Fig. 4. Equivalent circuit (a) and operation of astable multivibrator function by using interconnecting technique (b).

Here, we describe the role of the HPT-C (or HPT-D). HPT-C is not influenced by the optical feedback from the LDs and can be utilized for the initialization of the states to (0,0). For this purpose, the HPT-C is connected in parallel with LD1 and LD2. When the optical input is incident to the HPT-C, a part of the current flowing through the LD1 and the LD2 starts to flow to the HPT-C; this induces the reduction of the optical feedback from the LD1 to the HPT-A (or HPT-B) and from the LD2 to the HPT-E (or HPT-F) [8], and finally the optical feedback ceases and the flip-flop returns to the initial state.

From the above results, we may say that the ad-

 © 1997 COSiW SEP, Warsaw

vanced functions can be extracted from the philosophy that the higher the degree of integration, the higher the functionality of the device, and many kinds of functions can be achieved by making use of the optical and electronic couplings inside the OEIDs.

3. Toward multifunctinal OEIDs with surface-emission

3.1. Surface-emitting device with circular grating coupler embedded by crystal growth process

To apply the above flip-flop logical devices to two-dimensinal arrays, the surface-emitting element should be incorporated in the devices to tap the optical signals at desired positions. Here, we consider using the circular grating coupler as the surface-emitting element as described in Section 1. The circular grating coupler has the following advantages: 1) a very narrow symmetric beam divergence angle can be achieved by a wide emission aperture and 2) a good single longitudinal mode operation is obtained when the coupler is incorporated close to an active layer of a semiconductor laser.

In this section, we investigate the surface-emitting laser with an embedded circular grating coupler for possible application to optoelectronic integrated devices. Very few reports are available on devices with embedded circular grating couplers. The over-grown process on the grating coupler is considered very important to achieve multi-functional integrated surface-emitting devices since a smooth surface is required for the further fabrication process and integration as seen in Section 2-1. In the following, the fabrication of the circular grating coupler, its incorporation to the device, and the characteristics are described.

The circular grating coupler was fabricated by electron-beam (EB) lithography and reactive ion-etching (RIE). A SiN_x mask with 50nm thickness was deposited by plasma-assited chemical vapor deposition on a p-InP substrate and the EB resist (ZEP520) was spin-coated on it. A circular grating pattern with the period of 0.4 μm was drawn on the resist from the 20 μm to 120 μm region from the center by the EB. Then the SiN_x mask was etched through the resist mask by the RIE using CF_4 + O_2 gas, and successively the InP substrate was etched through the patterned SiN_x mask by the RIE using CH_4 + H_2 gas. The gratings formed thus on the InP substrate are shown in Fig. 5 (a), and a uniform circular grating coupler with a period of 0.4 μm and a depth of 0.15 μm was formed.

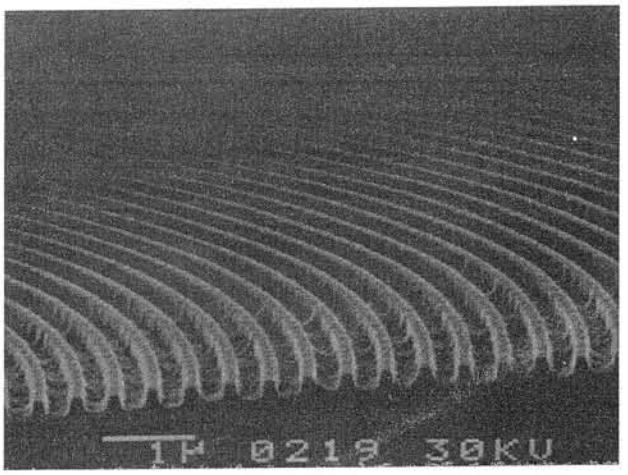

(a)

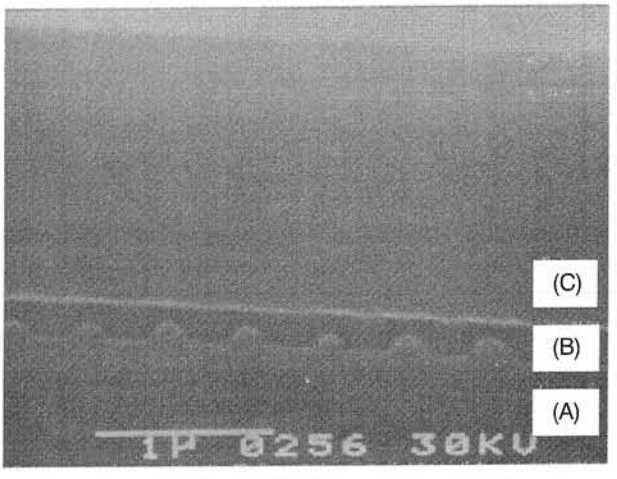

(b)

Fig. 5. (a)Circular grating coupler formed on InP substrate and cross-section of the grating coupler embedded by InGaAsP and InP layers: (A) InP substrate, (B) InGaAsP guiding layer, and (C) InP cladding layer.

After the SiN_x mask was removed, the circular grating on the p-InP substrate was embedded by an undoped InGaAsP active layer with the wavelength of 1.32 μm at room temperature and an n-InP cladding layer, which were grown by liquid phase epitaxy at 620°C with super saturation of 10°C Figure 5(b) shows an example of the cross section of an embedded grating coupler. The grating depth was slightly decreased, and the shape was changed from rectangular to sinusoidal, which was due to the meltback effect. The height of the embedded grating was slightly lower in [110] than in [1$\bar{1}$0] due to the different effect of the crystalline orientation on the meltback. The method to solve this problem will be discussed in the next section.

In the next step the wafer was processed to the surface-emitting device as shown in Fig. 6. To examine

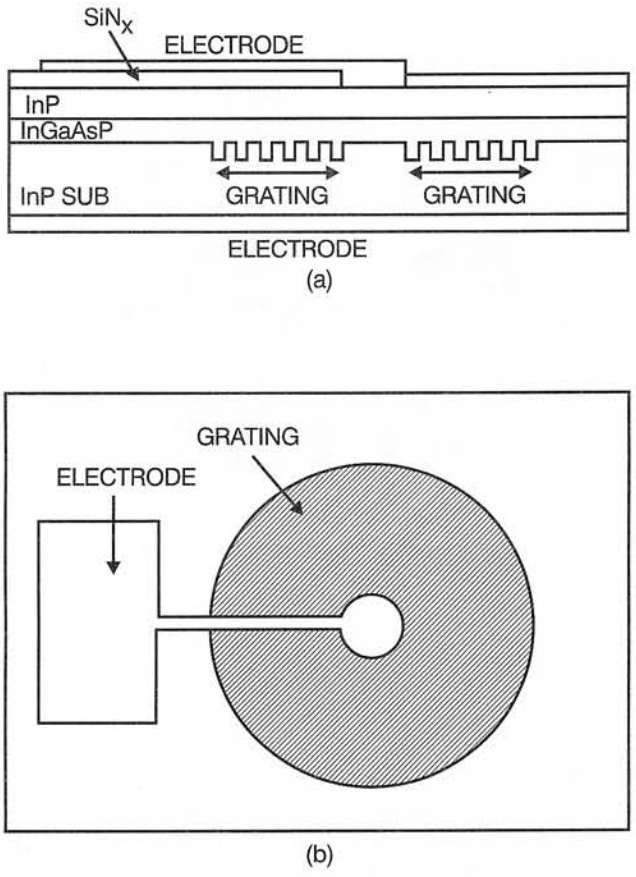

Fig. 6. Schematic structure of a surface-emitting device with embedded circular grating coupler: (a) cross section, (b) over-view.

the possibility of the operation of the gratings embedded in this way, we have utilized a relatively simple device structure without a current confinement structure nor a separate optical guiding layer. A current is injected to the central part within a circular grating coupler, where the SiN_x mask with the hole in the central part was formed on the wafer and the electrode was deposited on it as shown in Fig. 6. The device was bonded on a silver heat sink. For comparison, the device without the circular grating was also fabricated.

First of all, to examine the effect of the embedded circular grating, the electroluminescence spectra emitted to the direction normal to the substrate were measured for both devices with and without a circular grating. A distinct peak was observed at 1.34 μm for the device with a grating coupler at RT, which corresponds to the surface-emitting light deflected by the circular grating coupler. However, the peak wavelength was different from the designed value of 1.3 μm, and the deflected light power was not so strong but comparable with the spontaneous emission. This is due to the absorption loss at the grating coupler: the InGaAsP compositions of the grating coupler and the active current injection region are the same and much of the light emitted by the active region with the designed deflection wavelength of 1.3 μm was absorbed at the grating coupler before being deflected. To avoid this situation, we next cooled the device to 77K so that the absorption and the deflection wavelengths were separated. Figure 7 shows the electroluminescence spectra at 77K, where the current injection level was 50 mA, which is below the lasing threshold current. An emission, brighter by about 30 times, was observed in the wavelength region from 1.23 to 1.31 μm for the device with the grating coupler. It means that the spontaneous emission light propagating through the grating coupler is well-coupled out to the direction normal to the substrate surface. Figure 8 shows the near-field patterns of the devices with and without the grating coupler. For the device with a grating coupler, the diffracted light was observed in almost all region of the grating coupler. On the other hand, the emission from the device without a grating coupler was observed only around the electrode, where the emission is considered to be due to the current spreading into the passive region. Thus, it was found in these measurements that the absorption loss at the grating coupler region became very small at 77K.

After these fundamental examinations of the devices, we have measured the I-L characteristics of the device with the grating coupler. The measurement was done under continuous wave condition at 77K

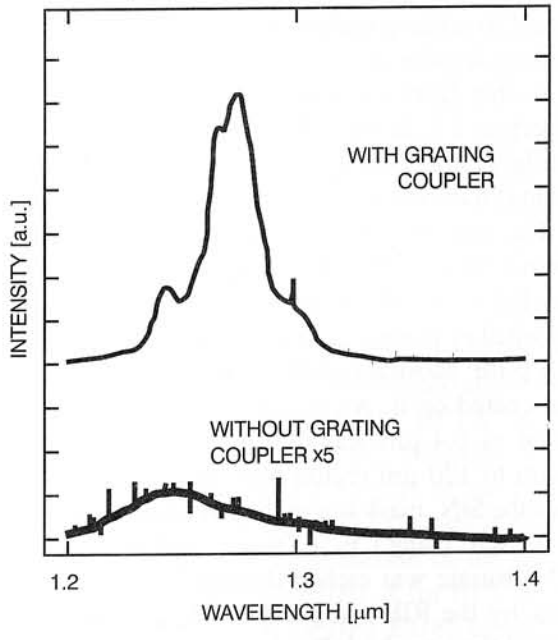

Fig. 7. Electroluminescence spectra emitted to the direction normal to the substrate surface from the device with and without a grating coupler at 77K.

 © 1997 COSiW SEP, Warsaw

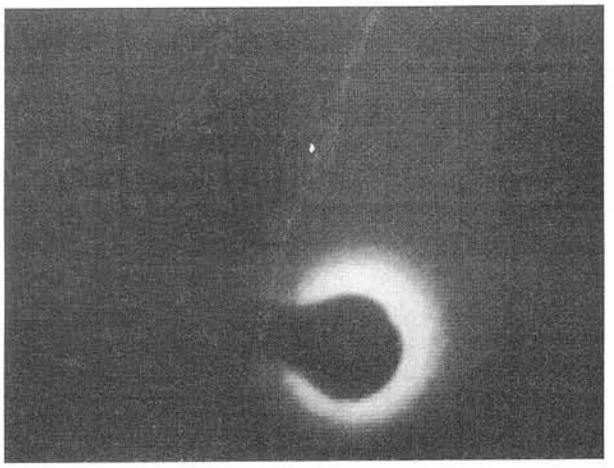

(a)

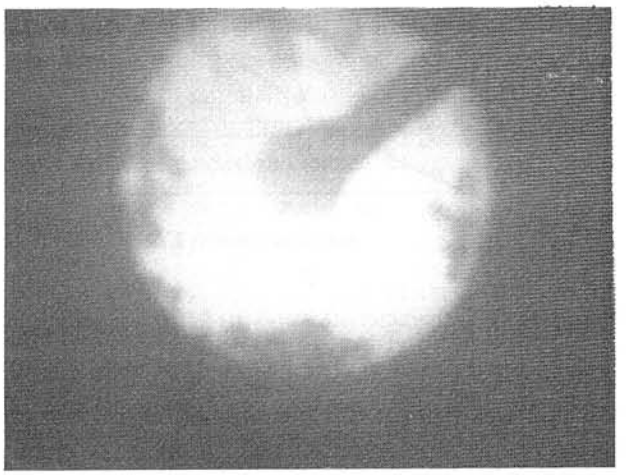

(b)

Fig. 8. Near-field patterns of the devices (a) with and (b) without circular grating coupler, where the bias current is below lasing threshold.

where the absorption loss at the grating cupler is well suppressed. Figure 9 shows the obtained result. Lasing oscillation has been achieved successfully, the threshold current was 264mA, and the measured maximum output power was 4mW. This is the first time that the lasing oscillation has been achieved with the embedded circular grating coupler, and it encourages us very much to achieve the multifunctional OEIDs with surface-emitting function. However, from the near-field pattern observation of the device, it was found that the lasing was observed mainly along the [110] direction and the pattern tended to spread into a wider area with increasing injection current. This behavior is due to a slight nonuniformity of the grating shapes in the azimuthal direction as described before.

To obtain the uniformity of the near-field pattern in the circular grating plane, it is very important to embed

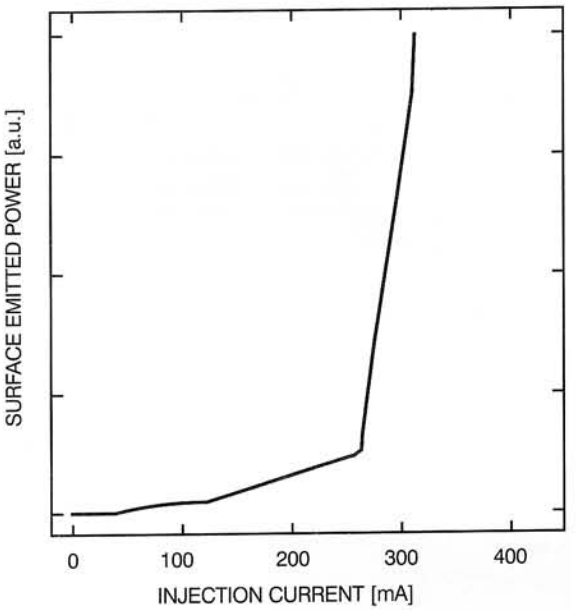

Fig. 9. I-L characteristics of the device with grating coupler under continuous wave condition at 77K.

the gratings uniformly, thus another embedding method in place of the LPE should be used. In the next section, the new method to embed grating will be discussed. Also, a multiple quantum well structure is introduced to achieve lower threshold current operation due to its higher differential gain and lower absorption loss at the grating coupler.

3.2. Embedding of gratings by mass-transport assisted wafer-fusion technique

We have recently proposed forming air/semiconductor gratings inside a semiconductor by wafer-fusion technique [10, 11] to solve the nonuniformity problem that occurs when the gratings are embedded by crystal growth process. Before applying it to the circular gratings, we have investigated the case of one dimensional gratings since this is the first trial to use the wafer-fusion technique to embed the gratings.

The basic idea for the device fabrication is shown in Fig. 10(a), where two epitaxial wafers A and B are stacked and fused. The wafer A has a separate confinement multiple quantum well (MQW) active layer, where the MQW is composed of seven periods of InGaAsP wells (λ =1.36 μm, thickness d = 7nm) and InGaAsP barriers (λ = 1.1 μm, d = 15 nm). The wafer B has a corrugated InP cladding layer and an InGaAsP etch-stop layer for the successive selective etching process. The wafers A and B were grown by MOVPE, and the second order diffraction gratings were formed

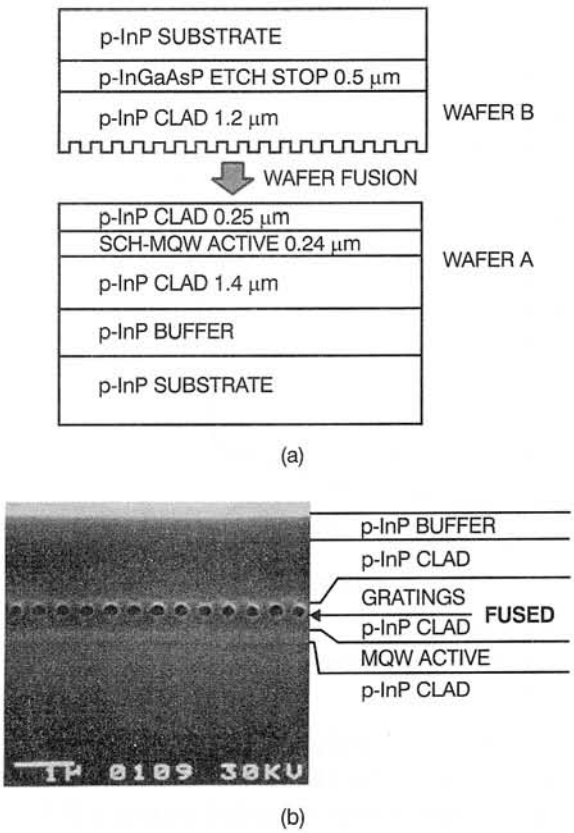

Fig. 10. (a) Schematic to show the basic idea for the device fabrication, (b) SEM cross sectional view of the device with fused air/semiconductor gratings.

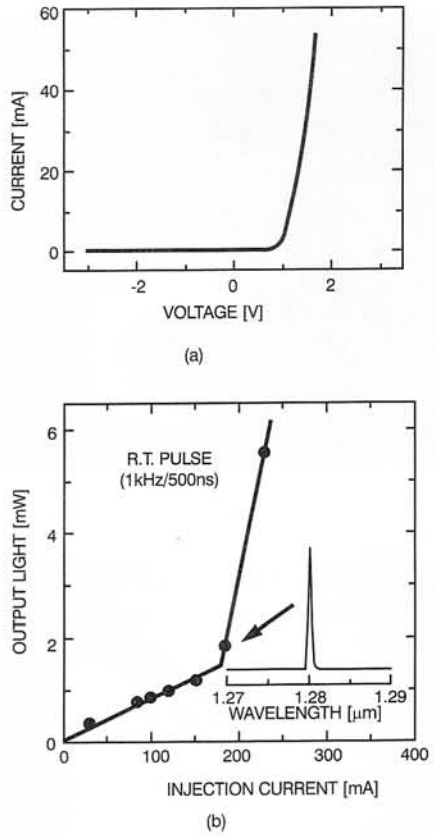

Fig. 11. (a) I-V characteristics and (b) I-L characteristics of the device.

on the wafer B by the electron beam lithography and reactive ion etching (RIE). Then, the surfaces of wafers A and B were pretreated by buffered HF solution, and the wafers were stacked under the pressure higher than 1.7N/cm^2 and heated in H_2 atmosphere. The wafer fusion conditions such as the temperature and the relationship of the surface orientations between wafers A and B were variously changed. Then, the wafers A and B were bonded as strong as to withstand various processes. Fig.10(b) shows the SEM cross sectional view of the sample. It is seen that the uniform air/semiconductor gratings were formed in the device having the depth and period about 0.2 μm and 0.4 μm, respectively. The rectangular-like grating shape obtained by RIE was changed to somewhat circular shape due to the mass-transport phenomenon. The fused interface becomes firmer and electronically more reliable with the aid of the mass-transport. It has been also found that the shape of the grating after wafer-fusion has almost no dependence on the crystalline orientation. This is very useful to apply the technique to the embedding of the circular gratings.

Then the InP substrate of the wafer B was etched off by the selective etching, and an electrode stripe laser structure was fabricated. Here, we note that the device has no lateral current confinement. A good I-V characteristic was obtained as shown in Fig. 11(a) for the device fabricated by the wafer-fusion condition: the fusing temperature was 620°C and the wafer orientation relationship between A and B was A//B = [110]//[1$\bar{1}$0]. Fig.11(b) shows the typical I-L characteristics of the device under pulsed condition at RT. Lasing oscillation has been successfully achieved, and the threshold current was I_{th}=170mA. When we consider the lateral current spreading due to lack of lateral confinement, the threshold current density can be estimated as low as 1.3kA/cm^2. The inset in Fig. 11(b) indicates the lasing spectrum at about I = I_{th}, and we can see that the device oscillated in a single longitudinal mode at 1.28 μm.

Since a device has a low loss MQW waveguide with second order diffraction gratings, it is expected that the light is coupled out normal to the substrate surface[12]. When a part of electrode was removed to form a grating output coupler as shown in Fig.12, the surface-emitted near-field patterns of the device became as shown in the figure. It is seen that the device works also as a grating-coupled surface-emitting laser.

Very recently, we have succeeded in the continuous wave oscillation of the DFB laser with air/semicon-

 © 1997 COSiW SEP, Warsaw

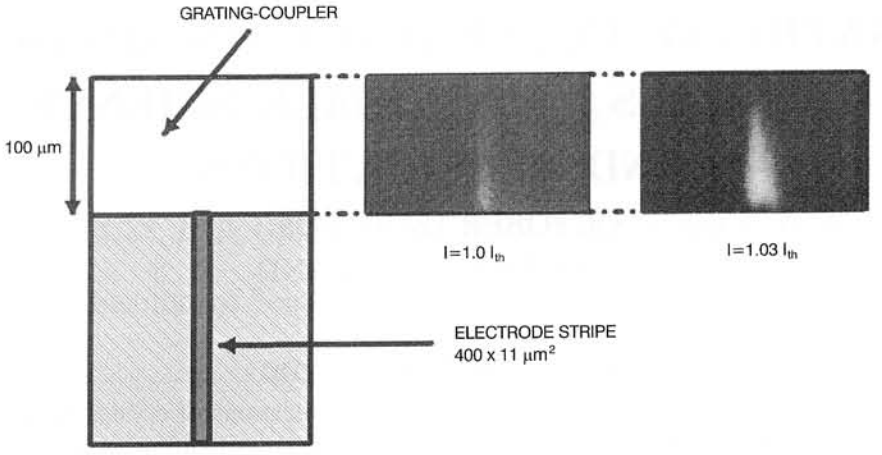

Fig. 12. Near-field patterns at 1.0 I_{th} and 1.03 I_{th} at room temperature emitted to the normal to the substrate surface.

ductor gratings embedded by wafer-fusion technique [13]. These results encourage us very much to apply the technique to circular grating coupled surface-emitting device. Now, we are trying to develop it, and the result will be reported in a near feature.

4. Summary

The new aspects of the OEIDs have been demonstrated by introducing an OEID composed of six HPTs and two LDs. The various advanced optical logical functions such as bistable, tristable, and astable flip-flops have been successfully demonstrated. These functions are based on the concept that the higher the degree of integration, the higher the functionality of the device with the aid of the internal optical and electrical couplings.

To let the OEIDs possess the surface-emitting capability without loss of the functionality, the method of introducing the surface-emitting element with embedded circular grating coupler has been described. The lasing oscillation has been successfully achieved. The new technology of wafer-fusion to construct an air/semiconductor grating has been also explained to obtain two-dimensionally uniform oscillation.

Acknowledgment

The authors would like to thank Dr. A. Wakahara, Messrs. T.Ishikawa and M.Imada. This work was partly supported by a Grant-in-Aid for Scientific Research from Ministry of Education, Science, Sports, and Culture of Japan and in part by the Matsuo Fundation.

References

1. A. Sasaki and M. Kuzuhara, Jpn. J. Appl. Phys. **20** (1981) L283.
2. A. Sasaki, Opto-Electronics Review **4** (1996) 1, and also see the references herein.
3. S. Noda and A. Sasaki, J. Fiber Integrated Opt. **12** (1993) 319, and see the references herein.
4. For example: S. Uchiyama, K. Iga, IEEE J. Quantum Electon. **QE-22** (1986) 301, and C.Chang-Hasnain, J.P.Harbison, C-E. Zah, M.W.Maeda, L.T.Florez, N.G.Stoffel, and T.P.Lee, IEEE J. Quantum Electron. **27** (1991) 1368.
5. C.M.Wu, M.Svilans, M.Fallahi, I.Templeton, T.Makino, J.Glinski, R.Maciejko, S.I.Najafi, C.Blaauw, C.Maritan, and D.G.Knight, IEEE Photon. Tech. Lett. **4** (1992) 960.
6. S. Noda, T. Ishikawa, M. Imada, and A. Sasaki, IEEE Photon. Tech. Lett. **7** (1995) 1397.
7. S. Noda, T. Katamata, K. Maehori, K. Shibata, and A. Sasaki, Optical Rev. **1** (1994) 213.
8. S. Noda, Y. Kobayashi, K. Shibata, and A. Sasaki, IEEE J. Quantum Electron. **31** (1995) 1465.
9. S. Noda, T. Takayama, K. Shibata, and A. Sasaki, IEEE Trans. Electron Devices **39** (1992) 305.
10. S. Noda, N. Yamamoto, and A. Sasaki, Jpn. J. Appl. Phys., **35** (1996) L909.
11. M. Imada, S. Noda, A. Sasaki, H. Kobayashi, and G. Sasaki, IEEE Photo. Tech. Lett. **9** (1997) 419.
12. S. Noda, K. Kojima, K. Mitsunaga, K. Kyuma, K. Hamanaka, and T. Nakayama, Appl. Phys. Lett. **51** (1987) 1200.
13. S. Noda, M. Imada, H. Kobayashi, and G. Sasaki, submitted to Conf. on Lasers and Electrooptics, San Francisco, USA, 1998.